Supplement of Biogeosciences, 12, 3579–3601, 2015
http://www.biogeosciences.net/12/3579/2015/
doi:10.5194/bg-12-3579-2015-supplement

Biogeosciences Open Access

Supplement of

Daily burned area and carbon emissions from boreal fires in Alaska

S. Veraverbeke et al.

Correspondence to: S. Veraverbeke (sander.veraverbeke@uci.edu)

Supplementary Table 1. Land cover aggregation scheme applied on Fuel Characteristic Classification System (FCCS) map (Ottmar et al., 2007). The numbers between brackets represent the FCCS codes.

black spruce
black spruce / lichen forest (85)
black spruce / feathermoss closed forest (87)
black spruce / sphagnum moss forest (88)
black spruce / sheathed cottonsedge woodland (89)
white spruce
white spruce forest (101)
white spruce - paper birch forest (103)
paper birch - trembling aspen - white spruce forest (105)
Sitka spruce -- western hemlock forest (322)
white spruce woodland (324)
white spruce -- mountain hemlock forest (325)
deciduous
paper birch - trembling aspen forest (93)
balsam poplar - trembling aspen forest (94)
trembling aspen / sagebrush boreal woodland (323)
balsam poplar -- paper birch forest (332)
tundra-grass-shrub
willow - alder shrubland (95)
cottongrass grassland (97)
marsh labrador tea - lingonberry tundra shrubland (98)
bluejoint reedgrass grassland (99)
Altai fescue grassland (100)
willow -- birch shrubland (326)
sedge -- shrub bog (327)
mountain heath tundra shrubland (329)
American dunegrass grassland (330)
Sitka alder -- salmonberry shrubland (331)
Dryas tundra shrubland (333)
Cassiope dwarf tundra shrubland (334)
sweetgale shrubland (335)
Alaskan tidal marsh grassland (336)
Alaskan freshwater marsh grassland (337)
Alaskan wet meadow grassland (338)
Alaskan herbaceous wet meadow grassland (339)
modified or managed xeric grass 1 (601)
non-vegetated
open water (911)
snow/ice (912)
developed-open space (921)

developed-medium intensity (923)
barren (931)
sparsely vegetated (933)
agriculture-cultivated crops and irrigated agriculture (982)

Supplementary Table 2. Location, year, depth of burn and carbon consumption of the field plots used in this study. (B: Boby et al. (2010), R: Rogers et al. (2014), T: Turetsky et al. (2011)). Depth of burn measurements were available for all sites. Direct estimates of belowground carbon consumption were available for the B and R plots. Direct estimates of aboveground carbon consumption were available for the B and R plots, with exception of one of the B plots. For the T data, belowground consumption was calculated using the soil-carbon accumulation curves per topographic class provided in Turetsky et al. (2011) (Figure S2) and is given between brackets. We used a digital elevation model (section 2.3.3) resampled to 450 m resolution for assigning the topographic classes to the field plots. Concave flat (slope ≤ 2%) areas were classified as lowland (L), convex flat areas were as upland (U). Sloped terrain was categorized as North (N) aspect (aspect ≥ 315° or < 45°), South (S) aspect (aspect ≥ 135° and < 225°), and East or West aspect (aspect ≥ 45° and < 135°, or ≥ 225° and < 315°).

latitude (°N)	longitude (°W)	fire year	depth of burn (cm)	belowground C consumption (kg/ m^2)	aboveground C consumption (kg/ m^2)	reference
66.31539	150.40571	2004	18.8	4.59	/	B
66.20925	150.27001	2004	11.6	0.95	0	B
66.21316	150.26391	2004	8	1.46	0.1	B
66.16861	150.20422	2004	12.3	4.53	0.4	B
66.16364	150.20207	2004	14.8	4.68	0.43	B
66.15127	150.18096	2004	14	4.58	0.39	B
66.14079	150.17242	2004	6.9	2.62	0.27	B
66.10976	150.15785	2004	8.7	3.39	0.45	B
66.10515	150.15355	2004	8.4	2.17	0.17	B
66.07446	150.16788	2004	7.2	2.95	0.16	B
66.07199	150.16674	2004	4.4	0.13	0.49	B
65.34931	146.66884	2004	14.2	2.82	0.29	B
65.35094	146.67092	2004	11.8	3.05	0.26	B
65.35313	146.67368	2004	10.1	3.56	0.18	B
65.1234	147.46541	2004	18	3.51	0.1	B
65.15298	147.48117	2004	10.2	0.8	0.1	B
65.15089	147.47616	2004	12.8	2.18	0.19	B
65.14843	147.47171	2004	19.6	2.15	0.1	B
65.15299	147.47819	2004	13.3	1.09	0.08	B
65.1424	147.4649	2004	18.7	4.37	0.48	B
65.14189	147.46556	2004	24.9	6.82	0.55	B
65.31961	146.71884	2004	5	1.69	0	B
64.3361	145.6895	2010	20.58	2.85	1.57	R
64.3391	145.7729	2010	20.26	1.82	0.67	R
64.3376	145.7697	2010	15.99	1.12	0.47	R
64.3352	145.778	2010	25.51	2.22	0.49	R
64.3379	145.6912	2010	18.15	2.13	0.77	R
64.3363	145.7046	2010	16.55	1.68	0.59	R
64.3357	145.7263	2010	22.14	2.51	0.84	R
64.3345	145.7304	2010	20.53	2.1	1.25	R

64.3358	145.7373	2010	25.42	3.18	0.93	R
64.3299	145.7329	2010	24.03	2.75	0.74	R
64.3344	145.7616	2010	11.78	1.59	0.4	R
64.334	145.7632	2010	8.8	0.85	0.15	R
64.3311	145.7511	2010	17.07	1.87	0.8	R
64.3289	145.7531	2010	18.5	1.32	1.01	R
64.3321	145.716	2010	17.1	1.9	0.96	R
64.3321	145.7117	2010	10.64	1.42	0.81	R
64.3353	145.7112	2010	9.78	2.17	1.09	R
62.69135	141.5316	2003	14	L (3.12)	/	T
65.60289	144.59124	2004	5.2	S (1.10)	/	T
65.52503	145.2483	2004	16	EW (2.90)	/	T
65.59183	144.66509	2004	21.7	L (5.82)	/	T
65.12033	147.43199	2004	19.8	N (4.64)	/	T
65.1164	147.42756	2004	24.3	N (5.92)	/	T
65.11822	147.42861	2004	21.5	N (5.12)	/	T
65.12245	147.43168	2004	28.3	N (7.09)	/	T
65.12361	147.43289	2004	15	EW (2.64)	/	T
65.35294	146.19033	2004	24.9	S (9.92)	/	T
65.33454	146.78486	2004	26.5	EW (6.12)	/	T
65.34025	146.72826	2004	25.7	S (10.36)	/	T
65.34	146.72	2004	13.5	S (4.20)	/	T
65.33924	146.70056	2004	13.2	S (4.07)	/	T
65.34652	146.66863	2004	12.6	S (3.81)	/	T
65.34354	146.68043	2004	16.1	S (5.38)	/	T
65.11629	147.42466	2004	27.9	N (6.97)	/	T
65.11974	147.4258	2004	26.5	N (6.56)	/	T
65.22076	147.13165	2004	7.9	S (1.98)	/	T
65.23367	147.13132	2004	28.3	EW (6.77)	/	T
65.14158	147.40933	2004	8.9	S (2.34)	/	T
65.14318	147.41279	2004	12.6	S (3.81)	/	T
65.35098	146.67121	2004	20.2	EW (4.10)	/	T
65.33582	146.75432	2004	13.8	S (4.33)	/	T
65.33695	146.78448	2004	11.4	EW (1.75)	/	T
65.3303	146.71143	2004	18	L (4.46)	/	T
65.34133	146.73332	2004	19.9	U (3.97)	/	T
65.1532	147.47236	2004	19.6	L (5.04)	/	T
65.15395	147.47608	2004	21.7	S (8.17)	/	T
67.0571	150.35113	2005	20.4	EW (4.16)	/	T
66.16383	150.20323	2004	21.7	S (8.17)	/	T
66.16169	150.19053	2004	17.1	S (5.85)	/	T
66.14033	150.17171	2004	12.5	L (2.66)	/	T
66.15354	150.1829	2004	15.5	L (3.61)	/	T

66.31301	150.39406	2004	16.5	EW (3.04)	/	T
66.10431	150.15702	2004	12.6	N (2.72)	/	T
66.185	150.9016	2004	15.3	S (5.01)	/	T
66.1827	150.21915	2004	19.3	EW (3.83)	/	T
66.21236	150.25108	2004	19.5	EW (3.89)	/	T
66.20321	150.2298	2004	24.7	EW (5.53)	/	T
66.19379	150.21366	2004	15.7	EW (2.82)	/	T
65.65362	149.07944	2003	6.3	N (1.20)	/	T
65.64965	149.0926	2003	12.4	N (2.67)	/	T
65.57709	148.94883	2003	6.5	EW (0.76)	/	T
65.57687	148.96002	2003	6.9	EW (0.83)	/	T
65.62037	149.09044	2003	8.6	N (1.73)	/	T
65.62163	149.0894	2003	15.9	N (3.58)	/	T
65.62382	149.0877	2003	15.7	N (3.53)	/	T
65.6232	149.08344	2003	17	EW (3.18)	/	T
65.61944	149.08718	2003	14	N (3.08)	/	T
65.61905	149.08413	2003	14.8	EW (2.58)	/	T
65.61845	149.08334	2003	10.5	EW (1.55)	/	T
65.61856	149.08218	2003	12	EW (1.89)	/	T
65.61984	149.08445	2003	14.8	EW (2.58)	/	T
65.57657	148.94145	2003	14.3	EW (2.46)	/	T
65.57617	148.94231	2003	17.5	EW (3.32)	/	T
65.62004	149.08567	2003	16.8	N (3.82)	/	T
65.61827	149.08567	2003	14.8	N (3.29)	/	T
62.83133	141.3446	2004	8.4	L (1.51)	/	T
64.39635	141.40998	2004	7.3	S (1.77)	/	T
64.39487	141.40833	2004	9.9	S (2.72)	/	T
65.30351	149.08207	2002	10.9	EW (1.64)	/	T
65.27854	149.02062	2002	18.1	EW (3.49)	/	T
66.79057	150.6909	2005	12.7	L (2.72)	/	T
66.65007	150.66595	2005	21.7	S (8.17)	/	T
63.24074	142.98912	2003	5.4	L (0.80)	/	T
64.88385	146.30439	2004	31.4	N (8.02)	/	T
64.88652	146.30662	2004	23.7	L (6.60)	/	T
64.90098	146.34856	2004	13.2	EW (2.18)	/	T
64.90023	146.35068	2004	12.4	EW (1.99)	/	T
64.89008	146.31987	2004	22.3	EW (4.75)	/	T
64.88198	146.30219	2004	31	EW (7.76)	/	T
64.88446	146.30585	2004	34.2	N (8.87)	/	T
64.88764	146.31305	2004	33	EW (8.51)	/	T
64.88784	146.30975	2004	30.4	L (9.41)	/	T
64.88728	146.31067	2004	32.2	L (10.21)	/	T
64.88513	146.30717	2004	30.6	L (9.50)	/	T

64.88329	146.30423	2004	33.4	N (8.63)	/	T
64.90092	146.35126	2004	5.3	EW (0.56)	/	T
64.90054	146.34386	2004	8.6	L (1.56)	/	T
64.9003	146.33406	2004	9.9	EW (1.42)	/	T
64.8918	146.31235	2004	14.6	EW (2.53)	/	T
64.88745	146.30784	2004	25.6	L (7.37)	/	T
64.88578	146.30284	2004	19	L (4.82)	/	T
64.88449	146.30113	2004	19.2	EW (3.81)	/	T
64.88518	146.30065	2004	21.3	EW (4.44)	/	T
64.08456	141.6474	2004	6.5	S (1.51)	/	T

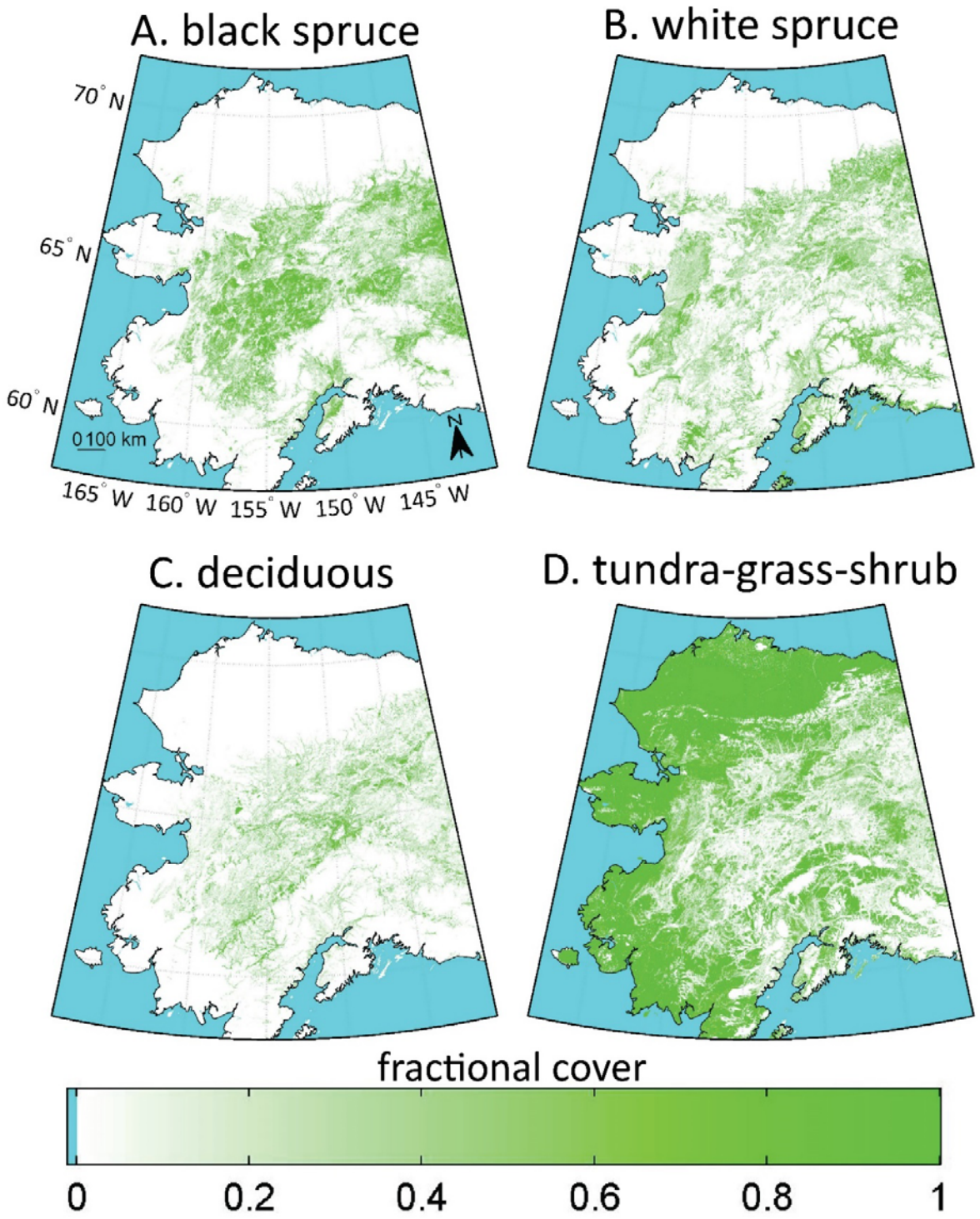

Supplementary Figure 1. Fractional cover maps of (A) black spruce, (B) white spruce, (C) deciduous trees and (D) tundra-grassland-shrubland. The maps represent the per-pixel fractional cover at 450 m of the aggregated land cover classes (Table S1) of the 30 m Fuel Characteristic Classification System (Ottmar et al., 2007) map for the year 2000.

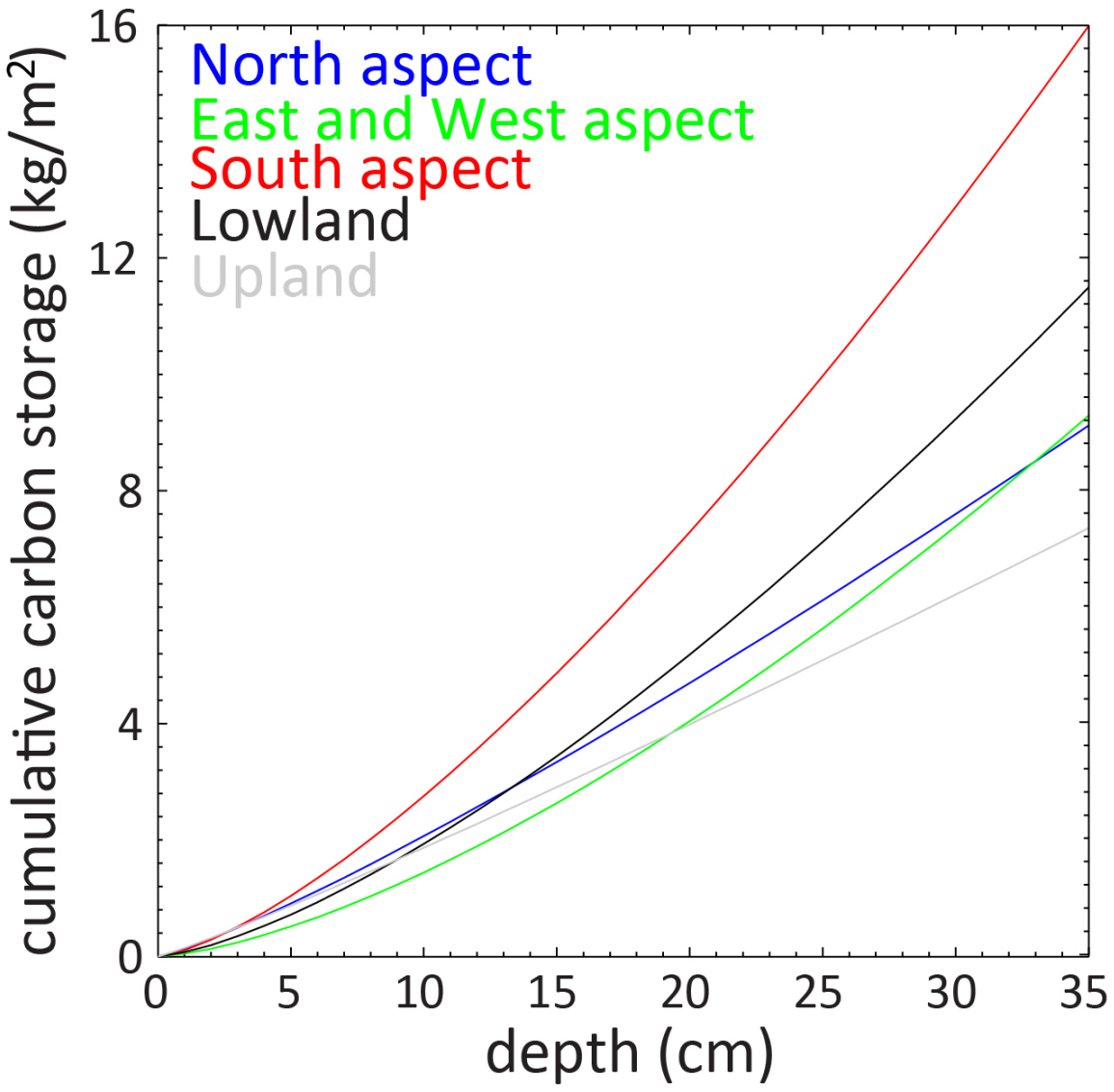

Supplementary Figure 2. Relationships between cumulative belowground carbon storage and depth for different topographic classes after Turetsky et al. (2011).

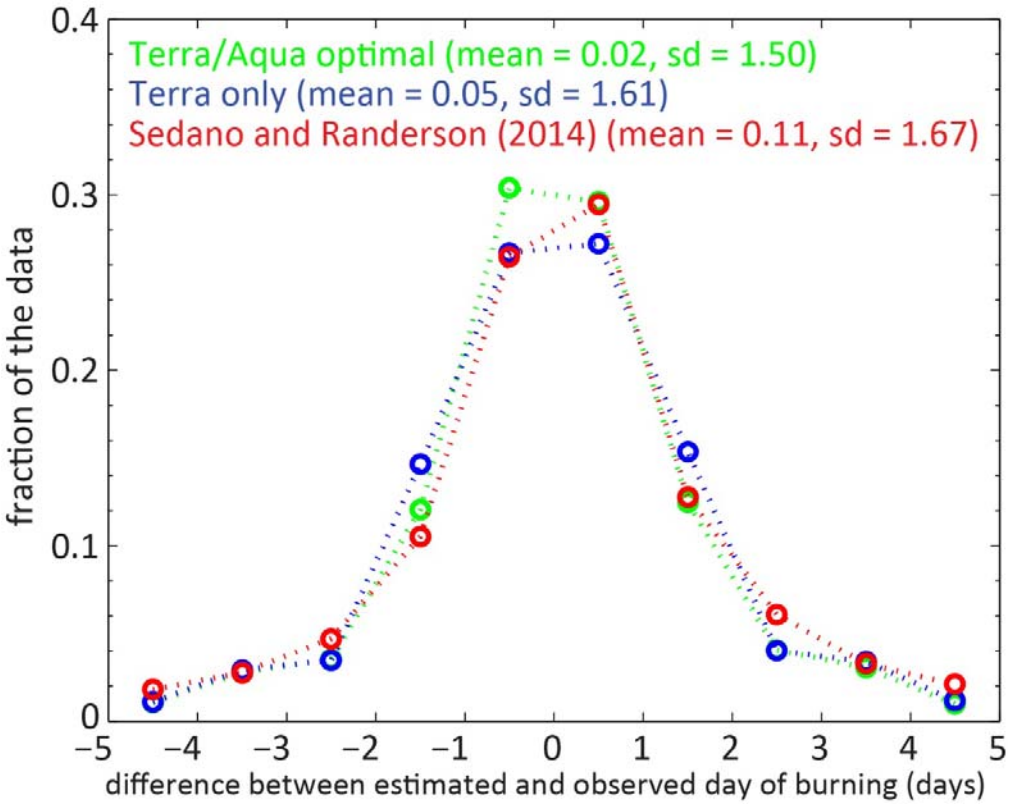

Supplementary Figure 3. Distribution of the difference between estimated and observed day of burning derived from the inverse distance weighting interpolation technique. The optimal setting for each pixel was defined by the value of the closest active fire detection with exclusion of active fire detections with scan angles higher than 40°. Sedano and Randerson (2014) did not exclude observations based on scan angle, considered a maximum of the ten closest pixels within a circular neighborhood with a 1 km radius, and used a weighting power of two for the interpolation. We used the large fire year of 2004 as subset for interpolation optimization. We varied three parameters in the optimzation: (1) the number of active fire detections considered to derive the day of burning for each pixel, (2) the weighting factor and (3) the threshold for exclusion of active fire detections with high scan angles. We varied the number of active fire detections included in the interpolation in steps of one between one and five, the power of the weigthing factor in steps of one between one and five and the exclusion threshold of scan angles in steps of 5° between 5° and 50°. For each combination of included active fire detections, weigthing power and scan angle exclusion threshold, we randomly selected 90% of the active fire detections for the progression interpolation. The remaining 10% was then used to validate the derived day of burning. We repeated this process ten times per combination in a fashion that every single active fire pixel had been nine times part of the interpolation dataset and one time of the validation dataset. We then used the mean and standard deviation of the distribution of the difference between the day of burning of the interpolation and validation dataset for each combination as quality indicator for the optimization. For the year 2001 of our study only Terra data is available, and we therefore repeated the optimal setting in a Terra-only scenario. Data is plotted in the middle of one-day interval boundaries on the x-axis. (sd: standard deviation)

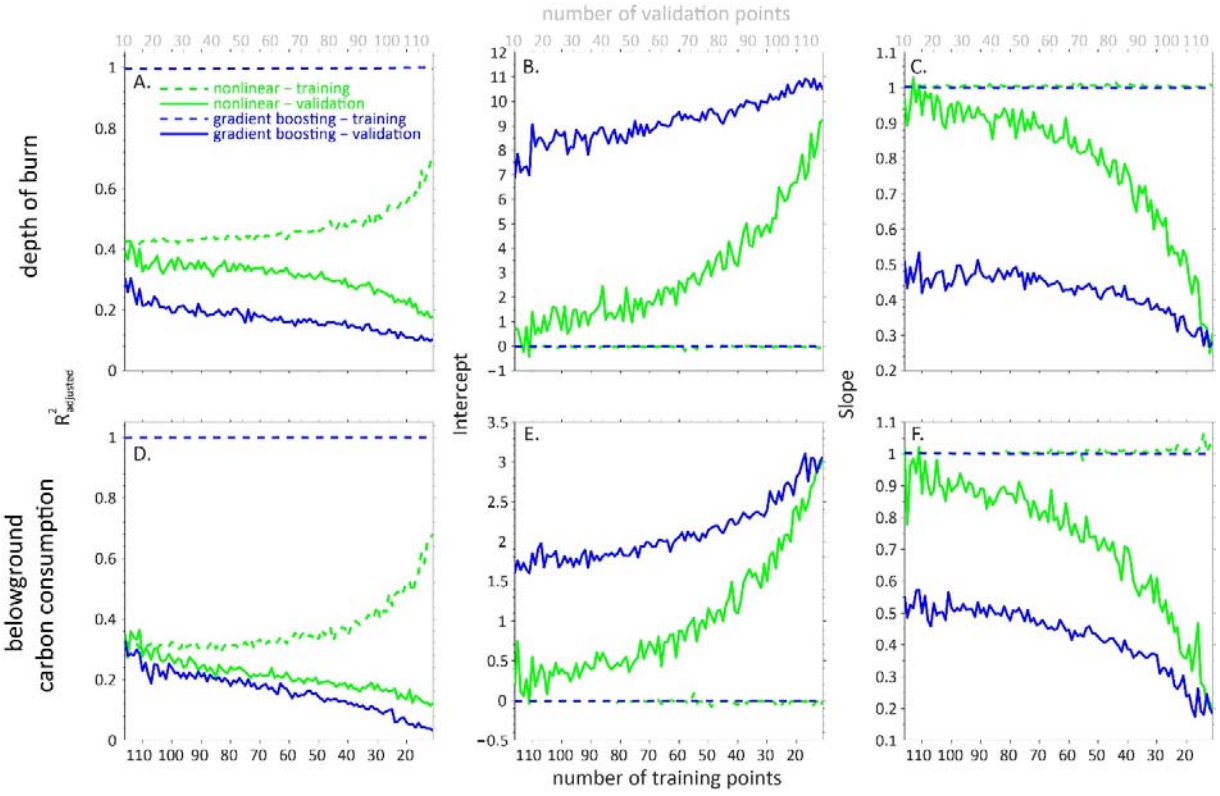

Supplementary Figure 4. $R^2_{adjusted}$, intercept and slope for the linear regression between observed and estimated values for training and validation plots in function of the number of training points for the depth of burn (A, B, and C) and belowground consumption model (D, E and F). To assess the robustness of the multiplicative nonlinear regression and gradient boosting techniques in our application to predict carbon consumption by fire in black spruce forests, we varied the number of field plots used as training data between 116 and 10, out of the total of 126 plots, in decreasing steps of one. The remainder of the plots was used for validation. For each combination of the number of training and validation plots, we randomly varied the selection of training and validation plots 100 times. For each combination and selection of training and validation plots, the prediction models were derived and applied on the validation data. The robustness for extrapolation of the models was then assessed as a function of the number of training plots by means of the $R^2_{adjusted}$, slope and intercept of the regression between estimated and observed values of the validation plots, averaged over the 100 random selections. While the gradient boosting technique revealed an apparent high performance ($R^2_{adjusted} \sim 1$) for the training plots alone, its performance for the validation plots was consistently lower compared to the nonlinear regression models. In addition, the intercept and slope values of the linear regression between observed and estimated values for the validation plots deviated substantially from the expect values of zero and one for the gradient boosting technique, while these regression lines followed more closely the 1:1 line for the nonlinear models when at least approximately 70 field points were used for training.

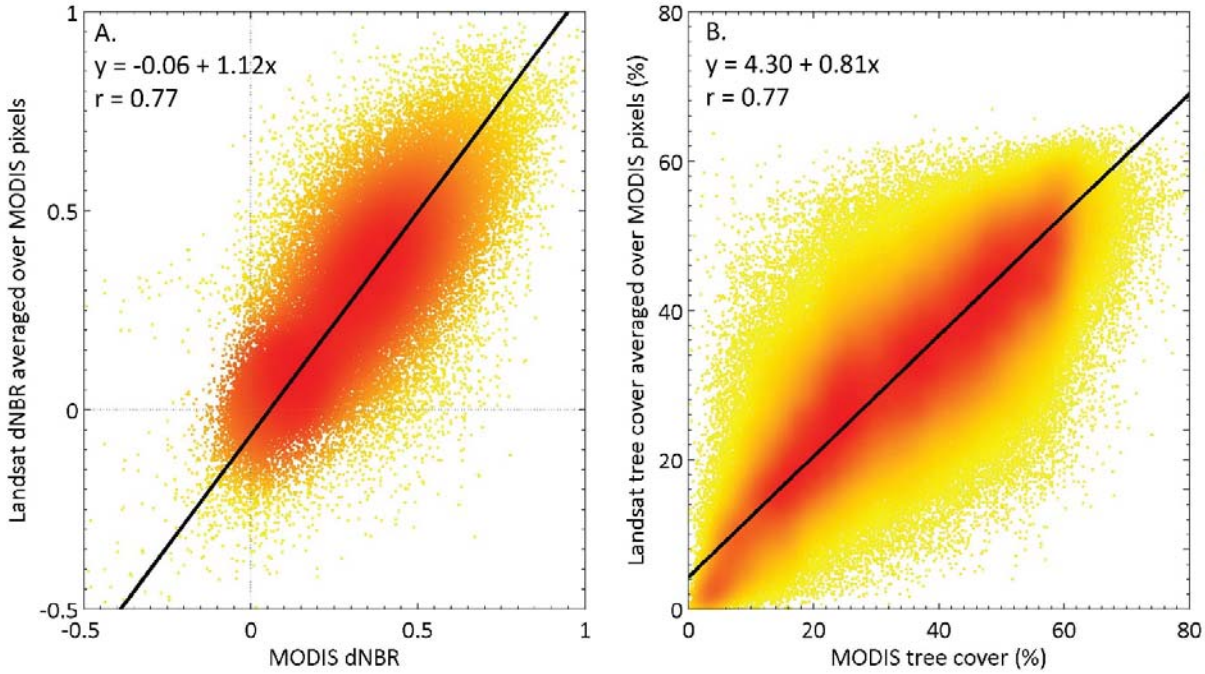

Supplementary Figure 5. Inter-sensor calibration between Landsat and the Moderate Resolution Imaging Spectroradiometer (MODIS) for (A) the differenced normalized burn ratio (dNBR) and (B) tree cover. For the dNBR comparison, all good-quality one-year post-fire observations of the large fire year 2004 from the Monitoring Trends in Burn Severity database (Eidenshink et al., 2007) were spatially averaged over MODIS pixels and compared with the corresponding dNBR values derived from the MOD13A1 product of 2004. For the tree cover comparison, all good-quality observations from the Landsat tree cover layer of the year 2000 (Sexton et al., 2013) that fell within the fire perimeters of the Alaskan Large Fire Database of the years 2001-2012 were spatially averaged over MODIS pixels and compared with the corresponding tree cover values of the MOD44B product of 2000. Type 2 regression was used to assess the linear relationship. Unexplained variability may originate from differences in assessment timing, view angle, illumination conditions, spectral response functions, and preprocessing methods between the Landsat and MODIS data.

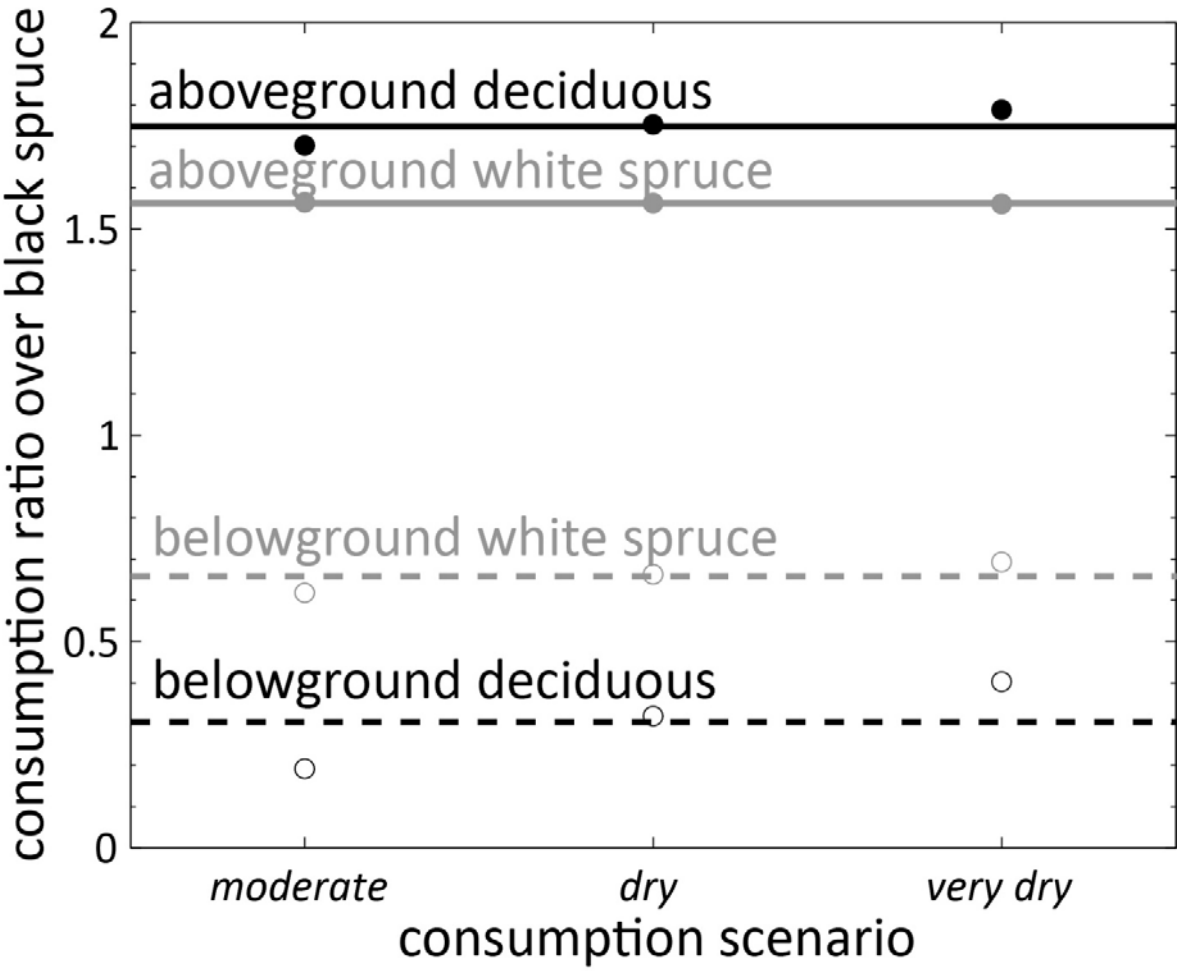

Supplementary Figure 6. Consumption ratios for above- and belowground white spruce/black spruce and deciduous/black spruce. Fuel consumption was estimated using Consume 3.0 (Ottmar et al., 2006) for black spruce (Fuel Characteristic Classification code 87), deciduous (93) and white spruce (101). Three consumption scenarios were applied: moderate (1000 h fuel moisture: 25%; duff fuel moisture: 60%, 10 h fuel moisture: 13%); dry (1000 h fuel moisture: 15%; duff fuel moisture: 40%, 10 h fuel moisture: 10%), dry (1000 h fuel moisture: 10%; duff fuel moisture: 20%, 10 h fuel moisture: 6%). In Consume 3.0 fuelbed type was defined as natural and we assumed 60 % canopy loading consumed (Prichard et al., 2006). Consumption ratios were relatively constant among the three different consumption scenarios and we therefore used the mean consumption ratio from these three scenarios.

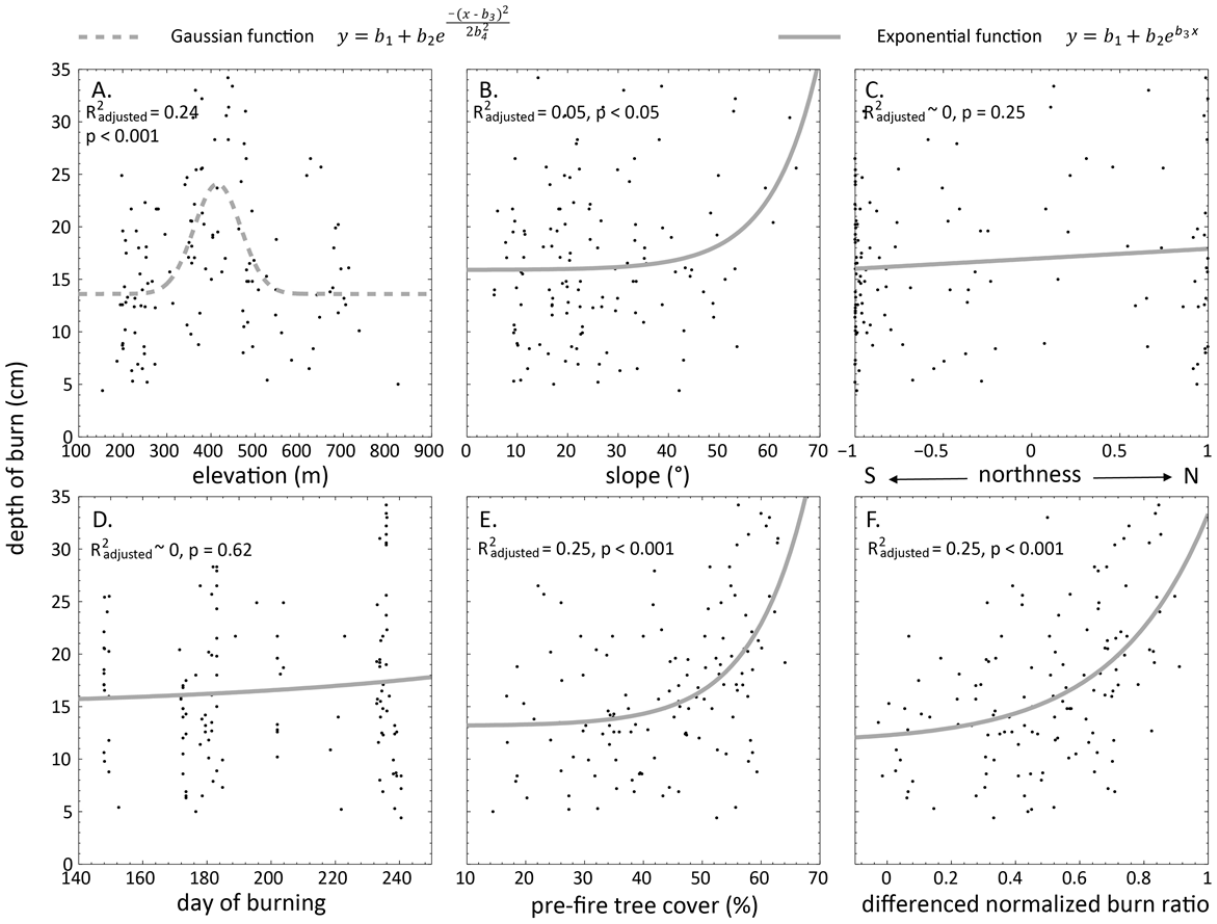

Supplementary Figure 7. Empirical relationships between the depth of burn from the field data and the environmental variables (n = 126). Depth of burn demonstrated a Gaussian response to elevation. The response function with the other variables was modeled as exponential.

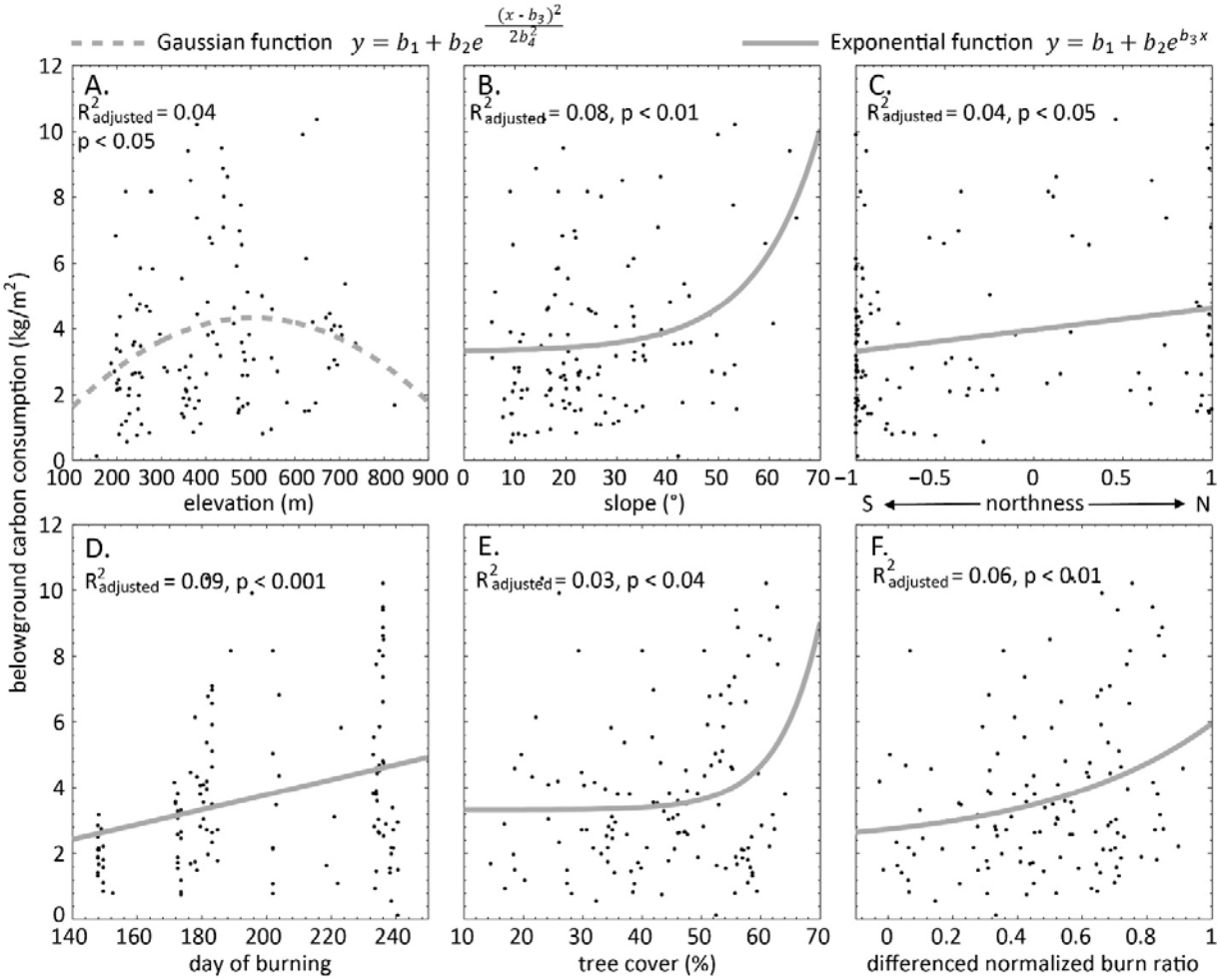

Supplementary Figure 8. Empirical relationships between the belowground carbon consumption from the field data and the environmental variables (n = 126). Belowground consumption demonstrated a Gaussian response to elevation. The response function with the other variables was modeled as exponential.

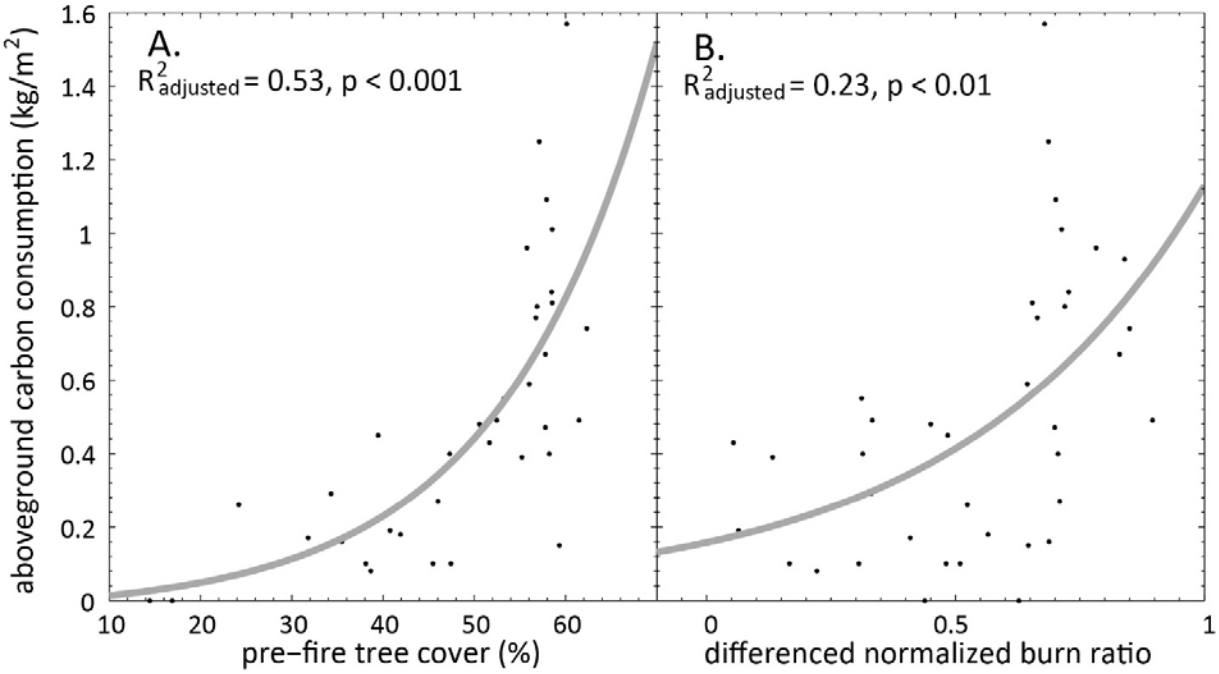

Supplementary Figure 9. Empirical exponential relationships between the aboveground carbon consumption from the field data and (A) the pre-fire tree cover and (B).the differenced normalized burn ratio (n = 38).

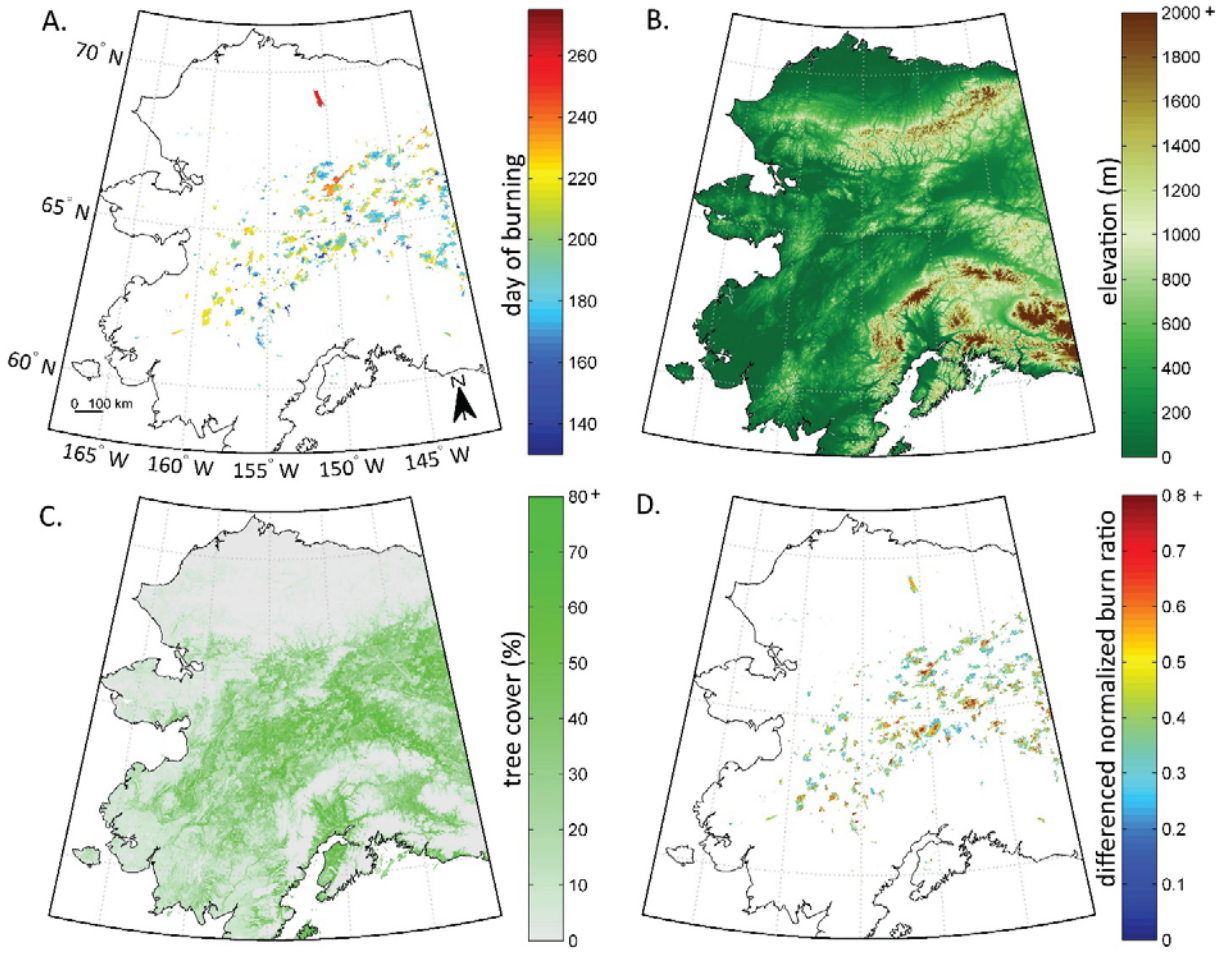

Supplementary Figure 10. Maps of (A) day of burning, (B) elevation, (C) tree cover and (D) differenced normalized burn ratio (dNBR) for the spatiotemporal domain of the study. The tree cover map of the year 2000 is shown. In the rare case a pixel burned more than once (< 1 % of the burned pixels), the average of the multiple burn observations was plotted for day of burning and dNBR.

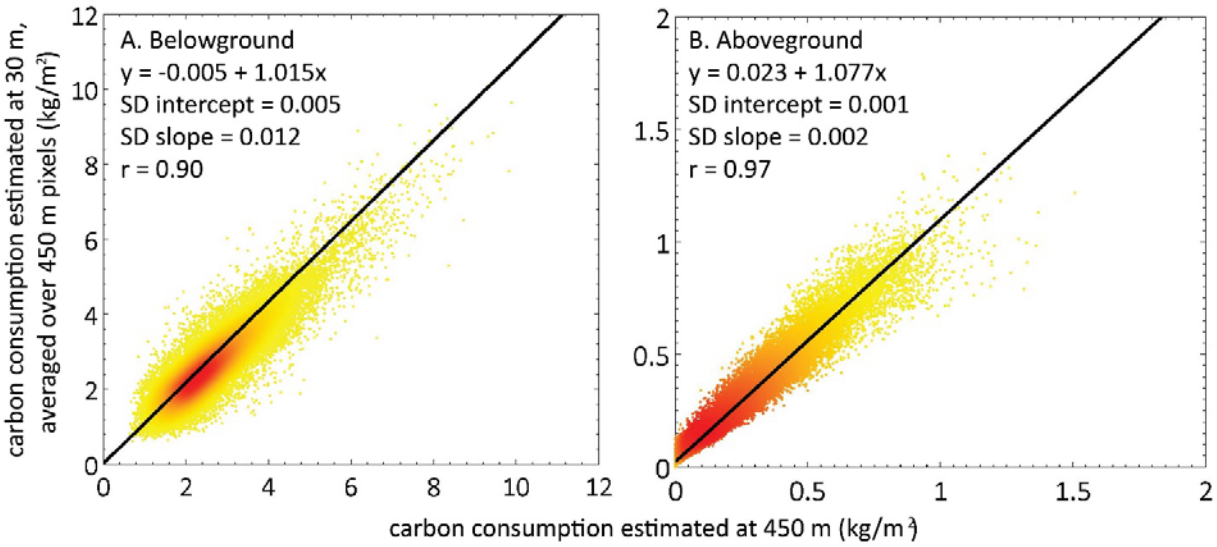

Supplementary Figure 11. Scatter plot and linear regression lines between carbon consumption estimated at 30 m resolution that were averaged over 450 m pixels, and carbon consumption estimated at 450 m based on 30 m input layers that were averaged over 450 m pixels. Both estimates use the same 30 m input layers (differenced normalized burn ratio, tree cover, elevation, day of burning and land cover classification). Type 2 regression was used to assess the linear relationship. The regression lines were used to correct for systematic bias resulting from applying a nonlinear model developed at 30 m resolution at 450 m resolution, and the standard deviation in slope and intercept fed into the uncertainty assessment.

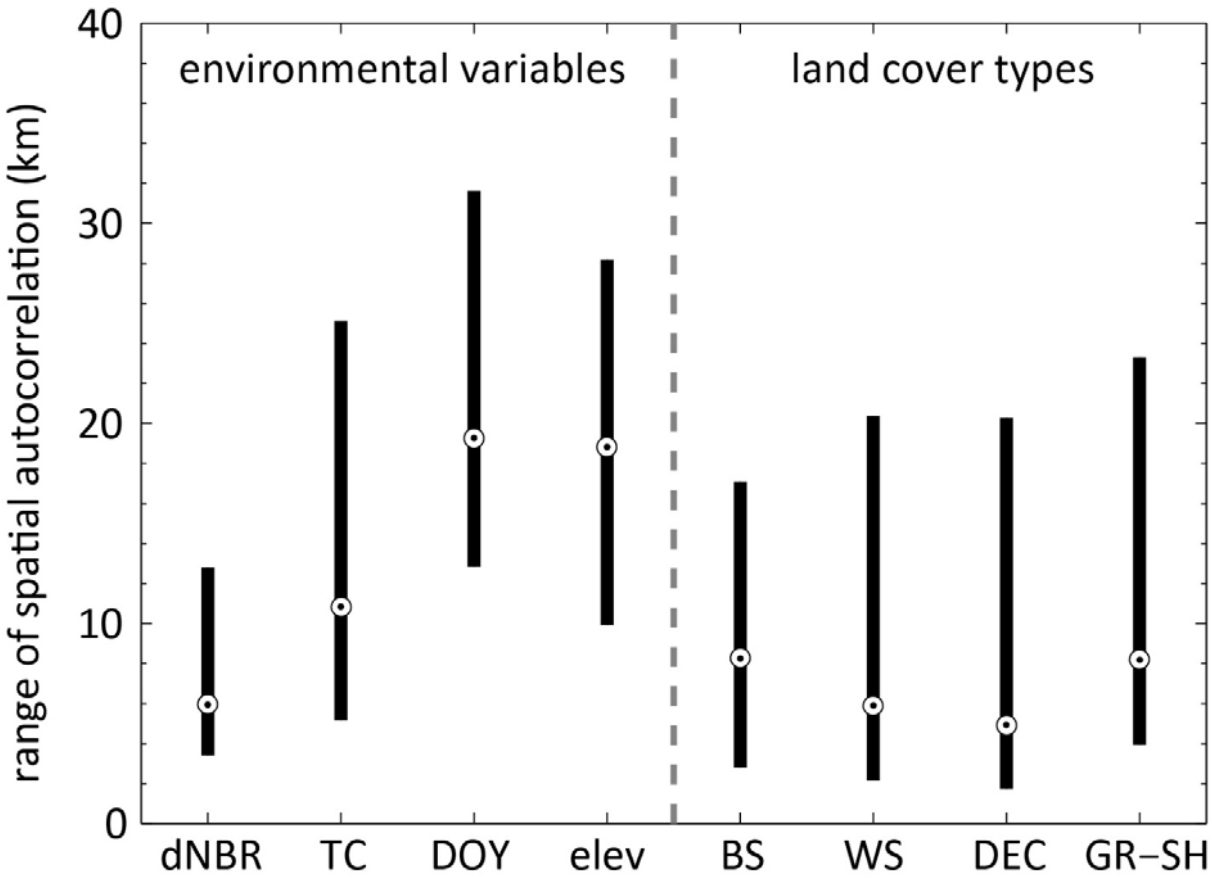

Supplementary Figure 12. Range of spatial autocorrelation of environmental variables and land cover types within all perimeters with a burned area larger than 10 000 ha. A spherical variogram fit was performed for all environmental variables and land cover types within these perimeters. The range of the variogram fit quantifies the degree to which variables are spatially correlated. At distances smaller than the range observations are spatially correlated, at distances larger than the range they are not. (dNBR: differenced normalized burn ratio, TC: tree cover, DOY: day of the year, elev: elevation, BS: black spruce, WS: white spruce, DEC: deciduous, GR-SH: grass-shrub).